Available online at www.sciencedirect.com

ScienceDirect

Natural Gas Industry B 3 (2016) 139–145

www.elsevier.com/locate/ngib

Research article

Impacts of bedding directions of shale gas reservoirs on hydraulically induced crack propagation☆

Sun Keming*, Zhang Shucui, Xin Liwei

School of Mechanics & Engineering, Liaoning Technical University, Fuxin, Liaoning 123000, China

Received 27 November 2015; accepted 16 March 2016
Available online 16 August 2016

Abstract

Shale gas reservoirs are different from conventional ones in terms of their bedding architectures, so their hydraulic fracturing rules are somewhat different. In this paper, shale hydraulic fracturing tests were carried out by using the triaxial hydraulic fracturing test system to identify the effects of natural bedding directions on the crack propagation in the process of hydraulic fracturing. Then, the fracture initiation criterion of hydraulic fracturing was prepared using the extended finite element method. On this basis, a 3D hydraulic fracturing computation model was established for shale gas reservoirs. And finally, a series of studies were performed about the effects of bedding directions on the crack propagation created by hydraulic fracturing in shale reservoirs. It is shown that the propagation rules of hydraulically induced fractures in shale gas reservoirs are jointly controlled by the in-situ stress and the bedding plane architecture and strength, with the bedding direction as the main factor controlling the crack propagation directions. If the normal tensile stress of bedding surface reaches its tensile strength after the fracturing, cracks will propagate along the bedding direction, and otherwise vertical to the minimum in-situ stress direction. With the propagating of cracks along bedding surfaces, the included angle between the bedding normal direction and the minimum in-situ stress direction increases, the fracture initiation and propagation pressures increase and the crack areas decrease. Generally, cracks propagate in the form of non-plane ellipsoids. With the injection of fracturing fluids, crack areas and total formation filtration increase and crack propagation velocity decreases. The test results agree well with the calculated crack propagation rules, which demonstrate the validity of the above-mentioned model.

Keywords: Shale gas; Hydraulic fracturing; Laboratory test; Bedding direction; Damage; Fracture initiation; Crack; Filtration; Extended finite element method

According to an IEA bulletin in August 2014, China had the largest recoverable shale gas reserves around the world, with technically recoverable resources up to 25.08×10^{12} m^3 [1]; however, the exploitation of shale gas in China remained in its initial stage, and its overall development was hindered by some technical and geological challenges [2]. Studies on fracturing rules of conventional reservoirs have made certain progress [3–6], but shale reservoirs [7–9] have complex bedding architectures, making their hydraulically induced cracks no longer plane ones [10]. Therefore, the hydraulic fracturing rules of shale gas reservoirs are different from those of conventional reservoirs, and the bedding direction of shale reservoirs has direct impacts on the propagation of hydraulically induced cracks. Available research results indicate that shale can be hypothesized to be a transverse isotropic medium [11,12]. Conventional hydraulic fracturing model assumes that cracks propagate in a predesigned plane. Alfano et al. [13] employed a cohesion model developed to study how cracks open along the joint plane. Based on the energy equation, Almia et al. [14] assumed that cracks propagated in the predesigned weak plane, and proposed the hydraulically induced quasi-static crack propagation variation model. In fact, however, cracks are generally three-

☆ Project supported by the National Natural Science Foundation of China "Stimulation to gas recovery from super-critical CO_2 multi-pulse gas-blasting low-permeability coals" (Grant No. 51574137).
* Corresponding author.
E-mail address: sskkmm11@163.com (Sun KM).
Peer review under responsibility of Sichuan Petroleum Administration.

http://dx.doi.org/10.1016/j.ngib.2016.03.008

dimensional, with complex shapes and random propagation paths. Common algorithms are generally limited in dealing with the propagation of complex cracks along random paths. Finite element method allows the cracks to cross the unit boundary and through the unit, and the complex-shaped cracks can be calculated in the regular grid without a given propagation path or redivision of the grid for the crack tips, which economizes calculation cost. Thus, it is the most effective method to deal with complex cracks. By rearranging extended finite element and virtual node freedom, Song et al. [15] used the superposition of unit and virtual node to describe the discontinuity. Du Xiuli et al. [16] and Zhang Qing et al. [17] discussed the application of extended finite element method and general extended finite element in dealing with cracks.

The authors selected several shale samples with different bedding directions for hydraulic fracturing test with the triaxial hydraulic fracturing test system. Based on the extended finite element method, the hydraulically induced fracture initiation criterion and the three-dimensional hydraulic fracturing model of shale gas reservoir were established to identify how the bedding direction affects the propagation of hydraulically induced cracks.

1. Hydraulic fracturing tests

1.1. Test schemes

Samples were taken in vertical and parallel bedding planes, with a size of 5 m × 5 m × 5 m. Before the test, an independently developed triaxial loading device was used to apply hydrostatic pressure on the sealed test-piece to simulate the formation stress. When the external load stabilized, the ISCO non-pulse high pressure pump was used to inject high-pressure liquid to the prepared borehole at a rate of 5 mL/min Table 1 shows the test scheme. Fig. 1 gives the schematic diagram of the hydraulic fracturing test scheme, and Fig. 2 shows the shale samples in vertical and parallel bedding planes.

1.2. Test results

Fig. 3 shows the variation of injection pressure along with time, and Fig. 4 shows the morphology of samples after fracturing. Accordingly, the following conclusions were drawn.

1) In Test 1, shale bedding is vertical to the minimum in-situ stress direction, and the induced cracks propagate along the bedding plane. As is shown on the fracturing curve, cracks are initiated at the eighth second and 9.87 MPa. The instantaneous initiation pressure declines and then rebounds. With the propagation of cracks, the injection pressure stabilizes at 6.5–7.0 MPa. At the thirty-second second, factures penetrate the entire sample, the injection pressure sharply declines, and liquid outflows from exit end of the sample.

Table 1
Test schemes.

No.	Axial pressure/MPa	Confining pressure	Bedding direction
1	10	6	Parallel
2	10	6	Vertical

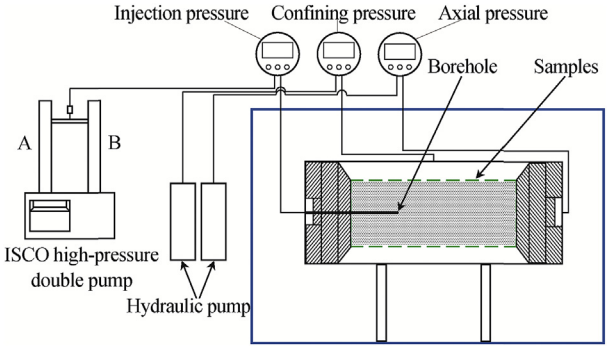

Fig. 1. Schematic diagram of the hydraulic fracturing test system.

a. Bedding parallel to borehole

b. Bedding vertical to borehole

Fig. 2. Shale samples before hydraulic fracturing.

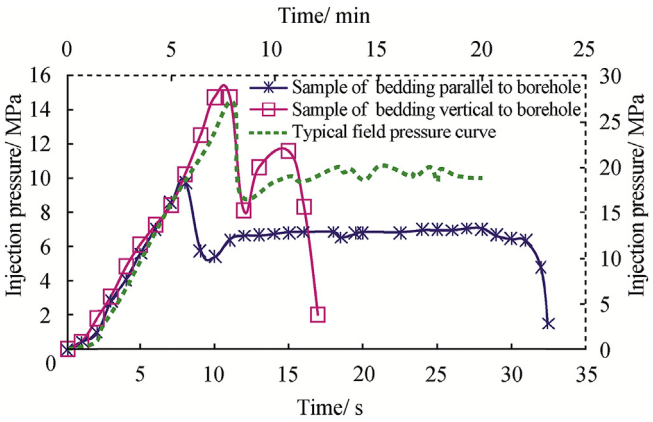

Fig. 3. Injection pressure vs. time in hydraulic fracturing.

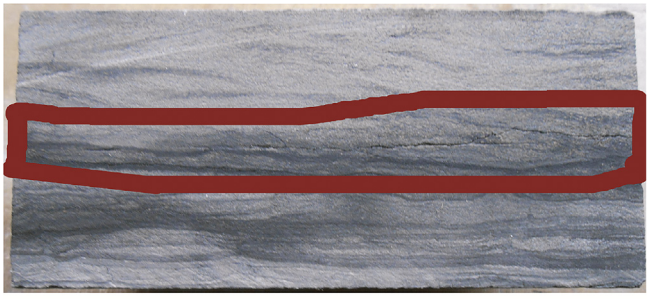

a. Bedding parallel to borehole

b. Bedding vertical to borehole

Fig. 4. Shale samples after hydraulic fracturing.

2) In Test 2, shale bedding is parallel to the minimum in-situ stress direction, and the induced cracks propagate along the bedding plane. Cracks are initiated at the tenth second and 14.8 MPa. Since the size in the bedding direction is small, cracks propagate only within a short time, under the pressure of 11–12 MPa.

2. Hydraulic fracturing model of shale gas reservoirs

2.1. Hydraulically induced fracture initiation model of shale reservoirs

The extended finite element method which uses the expansion function makes the discontinuous item included to describe the interruption, and the description of discontinuous field entirely isolated from the grid boundary. Thus, cracks will propagate along the random path. With the extended finite element method and UDAMINI, a subprogram of ABAQUS, the fracture initiation criterion was developed, which is suitable for cracks that initiate, propagate and convert in the random path in shale reservoirs. It is expressed as follows:

$$\begin{cases} f_{\mathrm{p}} = \langle \sigma^t_{\max} \rangle / \sigma^t_{\mathrm{c}} \\ f_{\mathrm{b}} = \langle \sigma^t_{\mathrm{b}} \rangle / \sigma^t_{\mathrm{bc}} \end{cases} \tag{1}$$

where, σ^t_{c} represents the tensile strength of material, Pa; $\sigma^t_{\max}$ represents the maximum tensile stress, namely, the principal stress, Pa; σ^t_{bc} represents the tensile strength of the material bedding, Pa; σ^t_{b} represents the normal tensile stress of the material bedding, Pa.

Zero is granted in the case of compressive stress, indicating that no cracking damage occurs at the time of compression, in other words, the symbol "< >" refers to the negative when it reaches zero. The initiation parameters $f = \max\{f_{\mathrm{p}}, f_{\mathrm{b}}\}$. When $f = 1$, fracture initiation starts; after that, f_{p} and f_{b} correspond to their respective law of evolution. The Power Law is employed for the crack evolution in correspondence to the fracture initiation criterion f_{p} for the maximum principal stress, namely,

$$G_{\mathrm{e}}/G_{\mathrm{eC}} = (G_{\mathrm{I}}/G_{\mathrm{IC}})^{a_{\mathrm{m}}} + (G_{\mathrm{II}}/G_{\mathrm{IIC}})^{a_{\mathrm{n}}} + (G_{\mathrm{III}}/G_{\mathrm{IIIC}})^{a_{\mathrm{o}}} \tag{2}$$

The BK Law is used for the crack evolution in correspondence to the fracture initiation criterion f_{b} for the bedding plane $G_{\mathrm{IIC}} = G_{\mathrm{IIIC}}$.

$$G_{\mathrm{eC}} = G_{\mathrm{IC}} + (G_{\mathrm{IIC}} - G_{\mathrm{IC}}) \left(\frac{G_{\mathrm{II}} + G_{\mathrm{III}}}{G_{\mathrm{I}} + G_{\mathrm{II}} + G_{\mathrm{III}}} \right)^{\eta} \tag{3}$$

where, G_{IC}, G_{IIC}, and G_{III} represent the release rate of Type I, II and III fracturing energy respectively; G_{I}, G_{II}, and G_{III} represent the release rate of Type I, II and III fracturing energy respectively; a_{m}, a_{n}, a_{o} and η represent material constants under the law.

2.2. Filtration model of hydraulic fracturing

The principle of effective stress, i.e. $\widehat{\sigma}_{ij} = \sigma_{ij} - \alpha_{ij} p_{\mathrm{p}}$, is fundamental for liquid–solid coupling. The flow pattern in rock matrix dovetails with the Darcy's law $V_{ij} = -(K_{ij}/\mu) \cdot \nabla p_{ij}$. In the fractured units, the liquid flows in a tangential pattern and normal leaching filtration. The tangential flow accords with the following expression:

$$v_{\mathrm{t}} = -(k_{\mathrm{t}}/\mu) \bullet \nabla p \tag{4}$$

where, v_t represents the tangential flow rate of fluid in the fracture, m/s; k_{t} represents the tangential permeability, m^2; μ represents the dynamic viscosity of fluid, mPa•s; ∇p represents the pressure gradient along the crack plane, Pa/m.

The normal filtration accords with the following expression:

$$\begin{cases} v_{\mathrm{p}} = c_{\mathrm{p}}(p_{\mathrm{i}} - p_{\mathrm{p}}) \\ v_{\mathrm{b}} = c_{\mathrm{b}}(p_{\mathrm{i}} - p_{\mathrm{b}}) \end{cases} \tag{5}$$

where, v_{p} and v_{b} represent the flow rate of liquid above and below the fracture, m/s; p_{i} represents the pore pressure of virtual node introduced, or the internal pressure, Pa; p_{p} and p_{b} represent the pore pressure above and below the fracture, Pa; c_{p} and c_{b} represent the filtration coefficient above and below the fracture, m/(Pa•s).

3. Calculation analysis

3.1. Calculation conditions

Reservoir depth is 1500 m. For easy observation of the propagation of cracks and avoidance of boundary size effect, the model was made with a size of 20 m × 20 m × 20 m, the borehole diameter (d) was taken as 0.15 m in the centre, and

the injection point was set in the centre of the simulated borehole (Fig. 5). Table 2 shows the calculation conditions, which are divided into two groups: (1) Conditions 1–7, with different in-situ stress and different bedding directions; (2) Conditions 4, 8 & 9, with different in-situ stress, and identical bedding directions. As to the material parameters, $E_p = 12$ GPa, $E_t = 9$ GPa, $G_p = 5$ GPa, $G_t = 3$ GPa, $v_p = 0.2$, $v_{pt} = 0.4$, $v_{tp} = 0.3$; the tensile strength limit of rock is 6 MPa, the tensile strength of bedding plane in shale reservoir is 0.5 MPa, the filtration coefficient is $6e^{-14}$ m/(Pa·s), the fluid viscosity is 2.5 mPa•s, the pump output is 0.36 m^3/min, and the fracturing time is 20 min. When the normal direction of the bedding (1-axis) is parallel to y-axis, the angle is zero; when it rotates counterclockwise, the angle becomes positive.

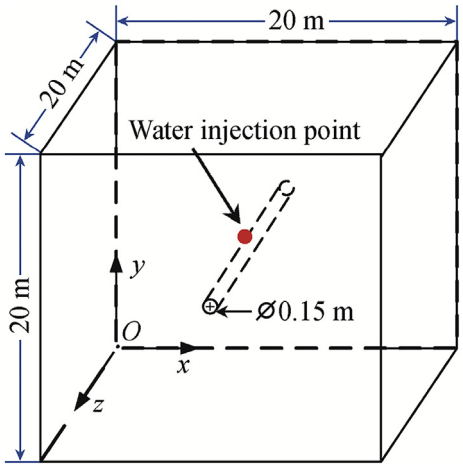

Fig. 5. Numerical model of hydraulic modelling.

Table 2
Calculation conditions.

Condition	Bedding direction/(°)	σ_x, σ_y, σ_z/MPa
1	0	10, 6, 25
2	15	10, 6, 25
3	30	10, 6, 25
4	45	10, 6, 25
5	60	10, 6, 25
6	75	10, 6, 25
7	90	10, 6, 25
8	45	10, 3, 25
9	45	10, 20, 25

3.2. Result analysis

Under Conditions 1–7, the angle between the normal direction of bedding and y-axis is 0°, 15°, 30°, 45°, 60°, 75°, and 90° sequentially. Cracks show three-dimensional non-planar extension (for example, Condition 5 in Fig. 6). For easily observing the relationship between the crack trending and the bedding direction or the direction of minimum in-situ stress, the orthographic projection is used (Fig. 7).

It is indicated in Fig. 7 that the direction of crack propagation is almost consistent with the bedding direction. As the angle between the normal direction of bedding and the direction of minimum in-situ stress increases, the angle between the crack propagation direction and the direction of minimum in-situ stress increases too. The simulating result dovetails with the test results, thus verifying the effectiveness of the hydraulic fracturing model.

The in-situ stress after hydraulic fracturing is the superposition of original in-situ stress, injection pressure and pore pressure increment caused by the seepage in the strata, and the existence of bedding plane makes the rock body represent homogeneity in all directions transversely. As for the weak strength of bedding plane, the propagation of hydraulically induced cracks depends on the state and strength of bedding plane after fracturing and the state and tensile strength of the stress in the minimum in-situ stress direction. If the normal tensile stress of the bedding plane firstly reaches the tensile strength of the bedding plane after fracturing, cracks propagate along the bedding plane; on the contrary, cracks propagate perpendicularly to the direction of minimum in-situ stress.

Compared with the results of the second group of conditions (4, 8 & 9), crack propagation direction is shown in Fig. 8. The ratio between the tensile stress in the direction of minimum in-situ stress and the limit of tensile strength is defined as the indicator n_1 of crack propagation vertical to the minimum in-situ stress, and the ratio between the normal tensile stress of the bedding and the limit of tensile strength in the bedding plane is defined as the indicator n_2 of crack propagation along the bedding plane.

As shown in Fig. 8-a, when the difference between vertical in-situ stress σ_y and the minimum horizontal in-situ stress σ_x (hereinafter referred to as in-situ stress difference) is 7 MPa, n_1 approximates to n_2, and non-planar crack propagation is obvious.

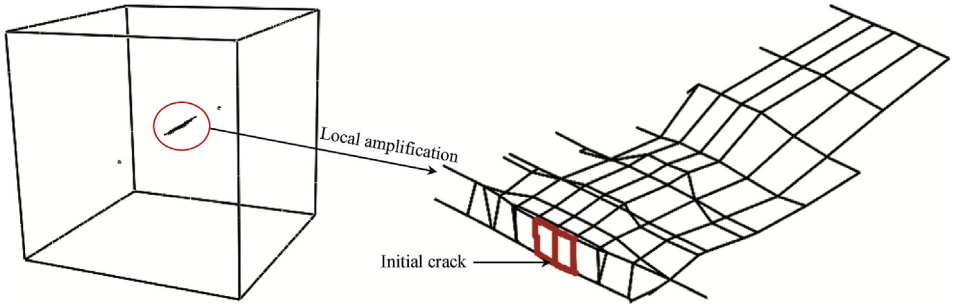

Fig. 6. Three-dimensional non-planar cracks in Condition 5.

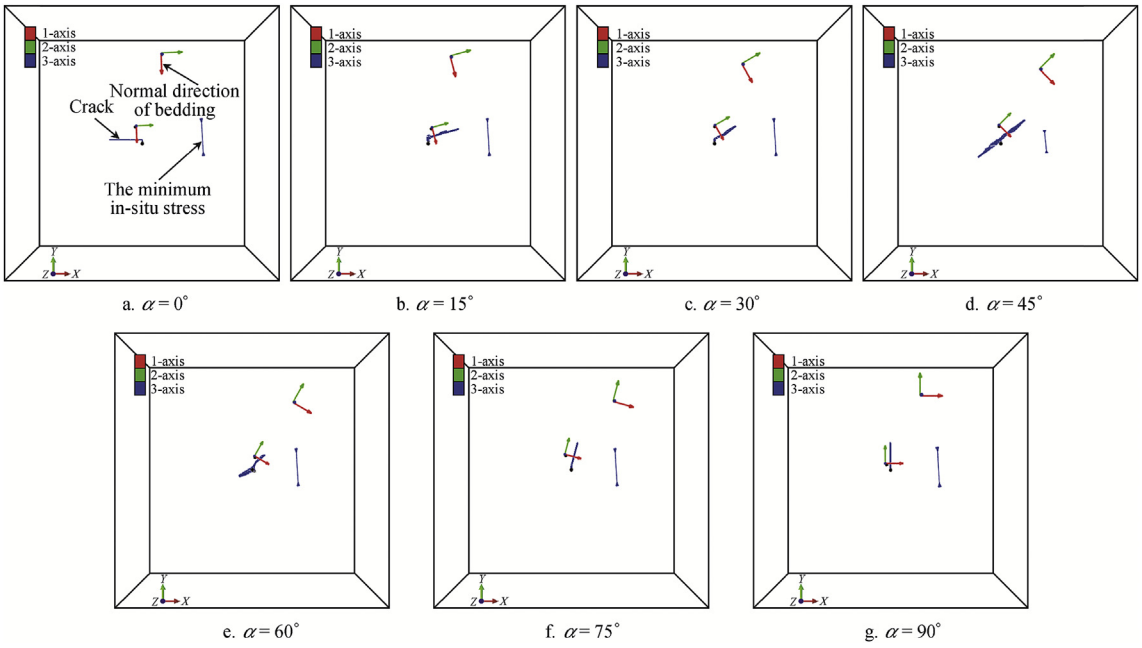

Fig. 7. Crack propagation under different bedding directions.

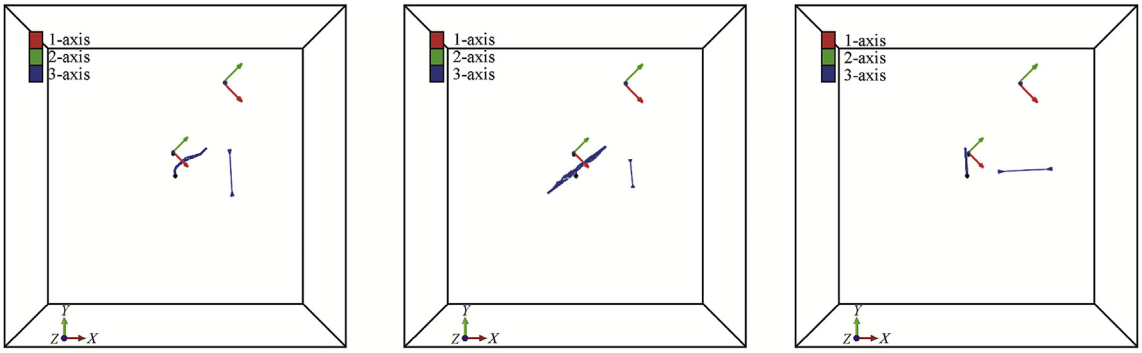

Fig. 8. Crack propagation under different in-situ stresses.

In the initial stage of crack propagation, n_1 is larger than n_2, and cracks propagate in a direction vertical to the minimum in-situ stress. As cracks further propagate, the pore pressure caused by liquid seepage and filtration increases, and n_2 increases to exceed n_1, and the crack propagation steers to the direction of bedding. As is shown in Fig. 8-b, when the stress difference is 4 MPa, n_2 is always larger than n_1, and cracks propagate along the bedding direction. On Fig. 8-c, when the stress difference is 10 MPa, n_1 is always larger than n_2, and cracks propagate in a direction vertical to the minimum in-situ stress.

According to the axial rotation expression, the normal stress of the bedding under original in-situ stress is expressed as:

$$\sigma_N = -\frac{1}{2}(\sigma_x - \sigma_y)\cdot\cos 2\alpha + \frac{1}{2}(\sigma_x + \sigma_y) - \tau_{xy}\sin 2\alpha \qquad (6)$$

Fig. 9 shows the changes of injection pressure for calculated σ_N, facture initiation pressure and crack propagation when $\tau_{xy} = 0$, $\sigma_x = 10$ MPa, $\sigma_y = 6$ MPa, $\sigma_N = 8-2\cos 2\alpha$, and $0° \leq \alpha \leq 90°$. It is indicated that the pressure for facture initiation and crack propagation and the normal stress increase with the increase of α, at a rate that increases and then decreases.

Fig. 10 shows the crack area and opening degree in different bedding directions. It is indicated that, given a constant displacement, as α increases, the pressure required for crack propagation increases, the crack propagation rate decreases; within the same time, the crack area decreases, and the opening degree increases.

Fig. 11 shows the variation of total filtration ratio and crack area with time in Condition 5. It can be seen that, as cracks propagate, the crack area expands, and total filtration ratio increases, and the expanding rate of crack area gradually decreases. Fig. 12 indicates the changes of crack propagation

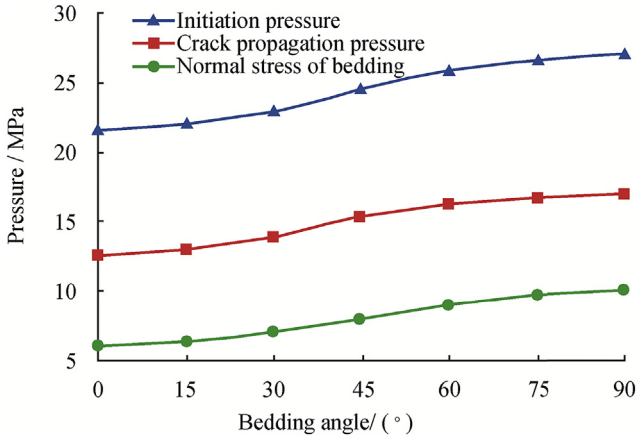

Fig. 9. Curves of pressure under different bedding directions.

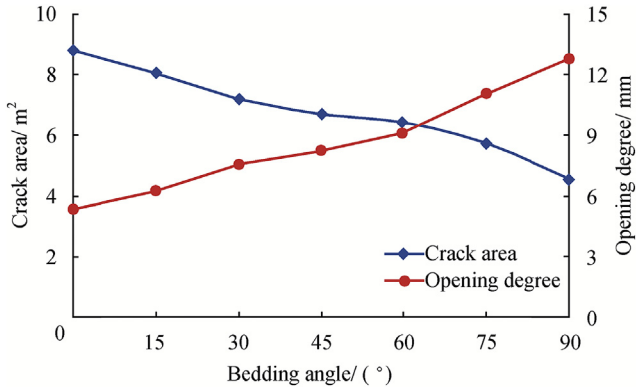

Fig. 10. Crack area and opening degree under different bedding directions.

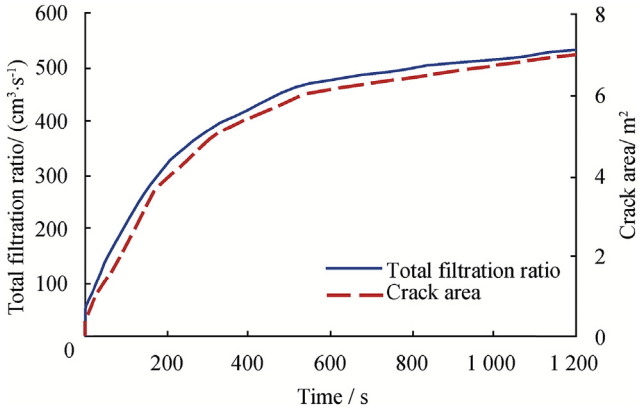

Fig. 11. Total filtration ratio and crack area vs. time.

in each stage obtained through calculation. Clearly, cracks present ellipsoidal non-planar propagation generally. In the initial stage of fracturing, in-situ stress concentration occurred around the borehole, which had significant influence on cracks, and the crack propagation turned to the normal direction of minimum in-situ stress. Away from the borehole, the in-situ stress concentration vanished, and the crack propagation changed to the direction of bedding. As the injection of fracturing fluid, cracks firstly propagated vertically from borehole wall to wellbore, and later along the borehole axis.

4. Conclusions

Through a comparison of the results of hydraulic fracturing test and three-dimensional numerical simulation of crack propagation in shale, it can be concluded as follows:

1) The agreement between simulated results and test results verifies the effectiveness of hydraulic fracturing model.

2) The hydraulically induced crack propagation rules of shale gas reservoir are jointly controlled by original in-situ stress and the strength and architectures of bedding plane. If the normal tensile stress of bedding firstly reaches the tensile strength of the bedding plane after fracturing, cracks will propagate along the bedding plane. If the tensile stress in the direction of minimum in-situ stress firstly reaches the limit of tensile strength, cracks will propagate in a direction vertical to the minimum in-situ stress.

3) Given a tensile strength of 6 MPa for the reservoir and a tensile strength of 0.5 MPa for bedding plane, the direction of bedding predominates the direction of crack propagation when the difference between vertical in-situ stress and minimum horizontal in-situ stress ($\Delta\sigma$) $\leq$ 4 MPa, and the state of in-situ stress predominates the direction of crack propagation when $\Delta\sigma \geq$ 10 MPa.

4) If factures propagate along the bedding plane, as the angle between normal direction of the bedding and the direction of minimum in-situ stress increases, crack area decreases, the opening degree of facture increases, and so does the pressure required for facture initiation and propagation. However, such pressure is the minimum when the direction of bedding is vertical to the direction of minimum in-situ stress.

5) Cracks present an ellipsoidal non-planar extension generally. With the propagation of cracks, the crack area increases, thus leading to an increase of total filtration ratio and the crack propagation rate decreases gradually.

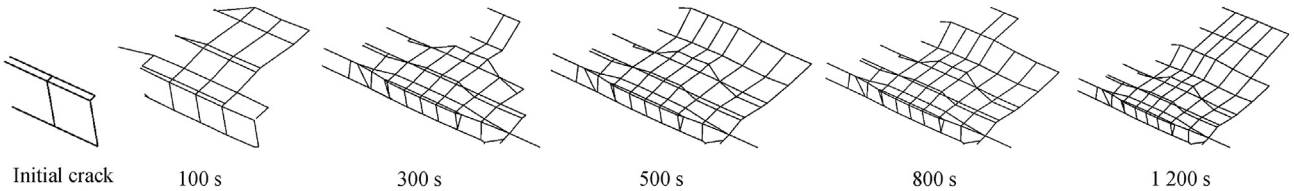

Fig. 12. Crack propagation in Condition 5.

References

[1] Yin Cheng, Gao Shikui, Dong Dazhong, Zhu Wenli, Wang Xinrui. Influencing factors for the development of shale gas industry. Nat Gas Ind 2015;35(4):117−25.

[2] Guan Xiaoxu, Yi Xiangyi, Yang Huohai. Contrast of shale gas reservoir conditions in China and the United States. J Southwest Petroleum Univ Sci Technol Ed 2014;36(5):33−40.

[3] Peirce A. Modeling multi-scale processes in hydraulic fracture propagation using the implicit level set algorithm. Comput Methods Appl Mech Eng 2015;283:881−908.

[4] Cheng Wan, Jin Yan, Chen Mian, Zhang Yakun, Diao Ce, Hou Bing. Experimental investigation on influence of discontinuities on hydraulic crack propagation in three-dimensional space. Chin J Geotechnical Eng 2015;37(3):559−63.

[5] Zhang Xiaodong, Zhang Peng, Liu Hao, Miao Shulei. Fracture extended model under hydraulic fracturing engineering for high rank coal reservoirs. J China Univ Min Technol 2013;42(4):573−9.

[6] Qian Bin, Yin Congbin, Zhu Juhui, Chen Xingyu. Research and practice of the impulse sand fracturing technology. Nat Gas Ind 2015;35(5):39−45.

[7] Lian Zhilong, Zhang Jin, Wang Xiuxi, Wu Heng'an, Xue Bing. Simulation study of characteristics of hydraulic fracturing propagation. Rock Soil Mech 2009;30(1):169−74.

[8] Sun Keming, Wang Song, Zhang Shucui. A numerical simulation on rules of facture extension during hydraulic fracturing in shale gas reservoir. J Liaoning Tech Univ Nat Sci 2014;33(1):5−10.

[9] Ma Tianshou, Chen Ping. Influence of shale bedding plane on wellbore stability for horizontal wells. J Southwest Petroleum Univ Sci Technol Ed 2014;36(5):97−104.

[10] Hou Bing, Cheng Wan, Chen Mian, Tan Peng, Yang Lifeng. Experiments on the non-planar extension of hydraulic fractures in fractured shale gas reservoirs. Nat Gas Ind 2014;34(12):81−6.

[11] Yang Jian, Fu Yongqiang, Chen Hongfei, Zeng Lixin, Li Jinshui. Rock mechanical characteristics of shale reservoirs. Nat Gas Ind 2012;32(7):12−4.

[12] Wang Qian, Wang Peng, Xiang Degui, Feng Yusi. Anisotropic of mechanical parameters of shale. Nat Gas Ind 2012;32(12):62−5.

[13] Alfano M, Furgiuele F, Leonardi A, Maletta C, Paulino GH. Mode I fracture of adhesive joints using tailored cohesive zone models. Int J Fract 2009;157(1):193−204.

[14] Almia S, Masoa GD, Toader R. Quasi-static facture growth in hydraulic fracture. Nonlinear Anal 2014;109:301−18.

[15] Song JH, Areias PMA, Belytschko T. A method for dynamic facture and shear band propagation with phantom nodes. Int J Numer Methods Eng 2006;67:868−93.

[16] Du Xiuli, Jin Liu, Huang Jingqi. Simulation of meso-fracture process of concrete using the extend finite element method. Chin J Comput Mech 2012;29(6):940−7.

[17] Zhang Qing, Liu Kuan, Xia Xiaozhou, Yang Jing. Generalized extended finite element method and its application in facture growth analysis. Chin J Comput Mech 2012;29(3):427−32.